



# Selective laser sintering scaffold with hierarchical architecture and gradient composition for osteochondral repair in rabbits



Yingying Du <sup>a, b, 1</sup>, Haoming Liu <sup>a, b, 1</sup>, Qin Yang <sup>a, b</sup>, Shuai Wang <sup>a, b</sup>, Jianglin Wang <sup>a, b</sup>, Jun Ma <sup>a, b</sup>, Insup Noh <sup>c</sup>, Antonios G. Mikos <sup>d, \*\*</sup>, Shengmin Zhang <sup>a, b, \*</sup>

<sup>a</sup> Advanced Biomaterials and Tissue Engineering Center, Huazhong University of Science and Technology, Wuhan 430074, PR China

<sup>b</sup> Department of Biomedical Engineering, Huazhong University of Science and Technology, Wuhan 430074, PR China

<sup>c</sup> Department of Chemical and Biomolecular Engineering, Seoul National University of Science and Technology, Nowon-gu, Seoul 139-743, Republic of Korea

<sup>d</sup> Department of Bioengineering, Rice University, P.O. Box 1892, MS-142, Houston, TX 77251-1892, USA

## ARTICLE INFO

### Article history:

Received 18 January 2017

Received in revised form

11 May 2017

Accepted 12 May 2017

Available online 12 May 2017

### Keywords:

Osteochondral defects

Selective laser sintering

Gradient microsphere scaffold

Hydroxyapatite

Poly( $\epsilon$ -caprolactone)

## ABSTRACT

Osteochondral defects cannot be adequately self-repaired due to the presence of the sophisticated hierarchical structure and the lack of blood supply in cartilage. Thus, one of the major challenges remaining in this field is the structural design of a biomimetic scaffold that satisfies the specific requirements for osteochondral repair. To address this hurdle, a bio-inspired multilayer osteochondral scaffold that consisted of the poly( $\epsilon$ -caprolactone) (PCL) and the hydroxyapatite (HA)/PCL microspheres, was constructed via selective laser sintering (SLS) technique. The SLS-derived scaffolds exhibited an excellent biocompatibility to support cell adhesion and proliferation *in vitro*. The repair effect was evaluated by implanting the acellular multilayer scaffolds into osteochondral defects of a rabbit model. Our findings demonstrated that the multilayer scaffolds were able to induce articular cartilage formation by accelerating the early subchondral bone regeneration, and the newly formed tissues could well integrate with the native tissues. Consequently, the current study not only achieves osteochondral repair, but also suggests a promising strategy for the fabrication of bio-inspired multilayer scaffolds with well-designed architecture and gradient composition via SLS technique.

© 2017 Elsevier Ltd. All rights reserved.

## 1. Introduction

Osteochondral defects caused by trauma, joint disease or aging severely impact the life quality of patients, due to the associated joint pain and impaired joint function [1,2]. Since cartilage is an avascular tissue with low cell density and metabolic activity, treatment of cartilaginous lesions remains a major challenge for orthopedic surgeons [3]. In addition, the complex hierarchical structure involving both articular cartilage and underlying subchondral bone is another huge challenge in reconstruction of osteochondral tissue. Several techniques are currently used to treat osteochondral defects, including autografts transplantation [4,5], autologous chondrocytes transplantation [6,7] and marrow

stimulation such as subchondral drilling [8] and microfracture [9]. Although successful in some aspects, each of these techniques has its own limitations. For instance, autografts transplantation suffers from donor site morbidity, incomplete integration and degradation of the graft tissue [10], while marrow stimulation results in fibrocartilage with inferior quality [11,12].

In recent years, tissue engineering emerged as a promising alternative for osteochondral regeneration [13–16]. Osteochondral defects involve multiple tissues, including the three articular cartilage layers (superficial, transitional and deep zone), calcified cartilage and subchondral bone. Biomimetic osteochondral scaffolds were thus required to repair multiple tissues simultaneously. Among these scaffolds, the biphasic scaffold model that combines a cartilaginous phase and a bony phase was the most common strategy [17–20]. Due to the limitations of fabrication techniques and scaffold structure, the issues of layer separation and weak interface bonding frequently occur, which affect cell migration, as well as long-term and complete osteochondral repair [18,21]. To overcome these limitations, an advanced selective laser sintering (SLS) technique was applied in this study to produce a bio-inspired

\* Corresponding author. Advanced Biomaterials and Tissue Engineering Center, Huazhong University of Science and Technology, Wuhan 430074, PR China.

\*\* Corresponding author.

E-mail addresses: [mikos@rice.edu](mailto:mikos@rice.edu) (A.G. Mikos), [smzhang@mail.hust.edu.cn](mailto:smzhang@mail.hust.edu.cn) (S. Zhang).

<sup>1</sup> These authors contributed equally to this work.

multilayer scaffold with a continuous hydroxyapatite (HA) gradient, which may be better suited for the regeneration of complex tissue interfaces. SLS is a rapid prototyping technique that has recently received a wide attention in creating diverse tissue scaffolds, mostly due to its advantages with high accuracy and customizability in manufacturing complex structures [22–24]. Compared with other 3D printing techniques, SLS employs a CO<sub>2</sub> laser beam to selectively sinter polymer or composite powders, producing porous scaffolds with high mechanical strength [25–27]. Consequently, SLS-derived scaffolds present a great potential for the integration of multiple properties, such as hierarchical structure from the cartilage layer to the subchondral layer, and adequate mechanical support for tissue repair.

In the current work, the poly( $\epsilon$ -caprolactone) (PCL) microspheres and the HA/PCL composite microspheres were used as building blocks of SLS to prepare a biomimetic multilayer scaffold for osteochondral repair (Fig. 1). PCL is one of the most commonly used polymers for bone and cartilage repair, with tailored biodegradable and mechanical properties [28,29], while HA is used to mimic the main mineral component of natural bone due to its excellent osteoconductive properties. Compared with the powder form used in conventional SLS strategies, microsphere-based SLS technique is utilized to enhance micro-scale porosity during the sintering process, which has been demonstrated by previous work [30]. The aim of this study is to verify the feasibility of using SLS to fabricate a gradient multilayer scaffold, and to assess its ability to repair osteochondral tissue in a rabbit model.

## 2. Materials and methods

### 2.1. Preparation and characterization of PCL microspheres and HA/PCL composite microspheres

The PCL microspheres and the HA/PCL composite microspheres

with 5 wt% to 30 wt% HA were separately prepared using a modified protocol of S/O/W emulsion solvent evaporation as previously described [30,31]. Briefly, PCL (Mw = 50,000) (Daigang Biomaterial Co., Ltd, China) was dissolved in dichloromethane. HA nanoparticles with the size distribution of 80–100 nm were synthesized using previously published protocol [32–34], and dispersed sufficiently in ethyl alcohol by ultrasonication. The two solutions were mixed sufficiently and added dropwise into a solution of 1.5% (w/v) poly(vinyl alcohol). After continuous stirring for 4–6 h, the microspheres were collected by centrifugation, washed and freeze-dried at –80 °C. The surface morphology, chemical structure and thermodynamic properties of the resultant microspheres were characterized by scanning electron microscope (SEM), Fourier transform infrared spectroscopy (FT-IR) and thermogravimetric analysis (TGA), respectively.

### 2.2. Design and fabrication of SLS-derived scaffolds

A cylindrical scaffold (4 mm in diameter, 2.8 mm in thickness) with pore size of 500  $\mu$ m was designed using a three-dimensional (3D) modeling software Pro/E and then exported into the STL format. The PCL microspheres and the HA/PCL composite microspheres were used as basic building blocks to fabricate the multilayer scaffolds using the SLS system (HRPS-IV, BinHu Mechanical & Electrical Co., Ltd, China). The HA content throughout the depth of the scaffold was designed to increase from 0 to 30 wt% with 5% increments from the top (articular cartilage) to the bottom (subchondral bone) layer, for a total of seven layers (Fig. S1). The sintering parameters were optimized for different microspheres in each layer, and were listed in Table S1. Also, the top PCL layer was set to be 400  $\mu$ m thick, which is close to the thickness of rabbit's articular cartilage. The continuous HA gradient was achieved by controlling the powder supply for each layer manually. Briefly, the PCL microspheres were first put on the work platform, spread out

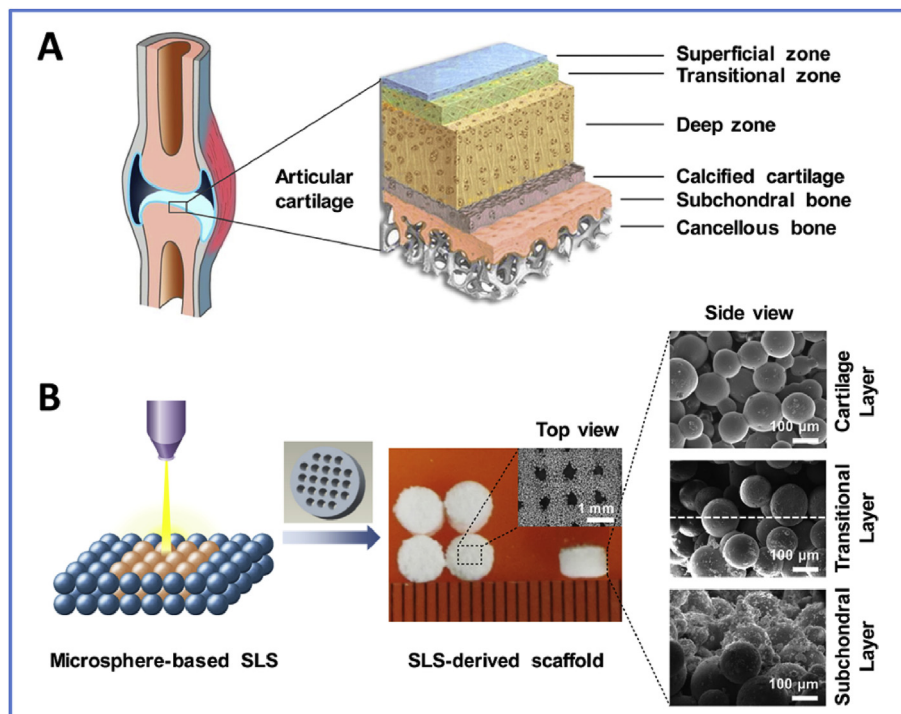


**Fig. 1.** Hierarchical architecture of natural osteochondral unit and its biomimetic replication in this work. (A) Natural osteochondral unit consists of several diverse tissue layers including superficial cartilage, middle calcified cartilage and deep subchondral bone, as well as transitional zones between different layers. (B) The PCL microspheres and HA/PCL composite microspheres were used as building blocks to fabricate bio-inspired multilayer scaffolds via SLS technique. The precisely-designed multilayer scaffold featured a macroporous cylinder with a continuous HA gradient from the articular cartilage layer to the subchondral bone layer.

by the roller and sintered for the top cartilage layer. By lowering the work platform, the rest of the layers having different HA content were continuously sintered with each layer having the same thickness of 400  $\mu\text{m}$ . The resultant scaffolds were termed as multilayer scaffolds. As a control, pure PCL scaffolds with the same dimensions were also fabricated via SLS layer-by-layer process, using only PCL microspheres, termed as PCL scaffolds.

### 2.3. Morphological characterization, porosity measurement and mechanical testing of scaffolds

Scaffolds were treated using a wind machine to remove unsintered microspheres attached to the surface or trapped in pores. Scaffolds were then examined by SEM to observe the morphologies of surface and longitudinal sections. The porosity of scaffolds was measured by a solvent replacement method as described elsewhere [35]. The unconfined compression tests of the scaffolds in dry state were tested on an electronic universal mechanical tester (Shimadzu AG-IC series, Shanghai) using a 0.1 kN load cell at a crosshead speed of 1 mm/min. The compressive modulus and compressive strength were separately calculated according to the stress-strain curve [36].

### 2.4. In vitro cellular evaluation of SLS-derived scaffolds

Rat mesenchymal stem cells (rMSCs, Cyagen Biosciences, USA) of passage 4–6 were used to evaluate the cytocompatibility of SLS-derived scaffolds. Briefly, the cells were cultured in Dulbecco's Modified Eagle Medium (DMEM), supplemented with 10% (v/v) fetal bovine serum, 1 mM glutamine and 1% (v/v) penicillin/streptomycin (all from Cyagen Biosciences, USA) in a humidified 5%  $\text{CO}_2$  incubator at 37 °C. The multilayer scaffolds were sterilized with  $^{60}\text{Co}$  gamma irradiation as described previously [30], washed twice with PBS, and subsequently immersed in complete medium overnight. The rMSCs were seeded on scaffolds at a density of  $5 \times 10^5$  cells/mL, and the culture medium was changed every 3 days. Cell adhesion on the multilayer scaffolds was separately observed by SEM and confocal laser scanning microscopy (CLSM; Olympus, FV500, Japan). Cell viability was evaluated by fluorescein diacetate/propidium iodide (FDA/PI) live/dead staining. Also, cell proliferation on the multilayer and the PCL scaffolds was measured by cell counting kit (CCK-8, Beyotime, China) after 1, 3, 5 and 7 days of culture, using tissue culture polystyrene (TCPS) as a control. Cell adhesion and alkaline phosphatase (ALP) activity on PCL and 5 wt%-30 wt% HA/PCL scaffolds were also performed respectively to investigate the effect of HA content on cell adhesion and differentiation.

### 2.5. Surgical procedure and scaffold implantation

A rabbit osteochondral defect model was created to evaluate the repair effect of the SLS-derived multilayer scaffolds *in vivo*. A total of 24 adult New Zealand rabbits (6-month-old) were used in this study. Briefly, the animals were anesthetized by an injection of 3.5% (w/v) pentobarbital sodium (1 mL/kg) into the ear-vein and randomly divided into three groups, namely multilayer scaffold, PCL scaffold and untreated control group ( $n = 8$  for each group). An osteochondral defect (4 mm in diameter and 3 mm in depth) was created using a sterile drill on each knee of the rabbits, resulting in 16 defects per group. During the surgical procedures, the defects were irrigated with saline solution to facilitate the drilling process and prevent the local overheating. Then the sterilized scaffolds were implanted into the defects, while the defects in control group were left untreated. Subsequently the incisions were closed with a degradable suture (5-0 silk suture, Ethicon, USA). A dose of 40,000 IU penicillin per animal per day was intramuscularly injected after the operation for 3 days. All procedures for animal experiments

were approved by the Institutional Animal Care and Use Committee (IACUC) of Huazhong University of Science and Technology.

### 2.6. Micro-computed tomography (micro-CT) analysis

The animals were euthanized to evaluate osteochondral repair by micro-CT, at 6 and 12 weeks post-surgery. The samples were harvested and fixed in 4% (w/v) buffered paraformaldehyde for 2 days, mounted in a poly(methyl methacrylate) holder, and subjected to micro-CT analysis using a Micro-CT 50 scanner (Scanco Medical, Switzerland). The samples were scanned with an X-ray beam energy of 70 kV, beam intensity of 109  $\mu\text{A}$ , and spatial resolution of 15  $\mu\text{m}$ . The final 2D images, composed of 1000 axial-cut slices, were loaded into 3D modeling software ( $\mu\text{-CT}$  Tomography V6.1-2) to quantify the architecture of the samples (e.g. bone volume, trabecular thickness). The threshold was set at 375 mg HA/ $\text{cm}^3$  to distinguish mature bone from the residual scaffold and soft tissue [37].

### 2.7. Histological evaluation

After the micro-CT analysis, the samples were decalcified in 15% (w/v) ethylenediamine-tetraacetic acid (EDTA), dehydrated through series of ethanol, embedded in paraffin, and longitudinally sectioned into slices with an approximate thickness of 5  $\mu\text{m}$  using a paraffin microtome (Leica EG 1160). The sections were subsequently stained with hematoxylin and eosin (H&E), safranin-fast green (S-F), toluidine blue (T-B) and Masson's trichrome (M-T) to observe new tissues. The histological sections were blindly and independently scored by three evaluators, using an established histological scoring system (Table S2) for osteochondral defects [38–40]. The scores were averaged to determine the final scores.

For immunohistochemical (IHC) staining of collagen type I (COL I), collagen type II (COL II), collagen type X (COL X), aggrecan (AGG) and osteocalcin (OCN), sections were immersed in 0.3% (w/v)  $\text{H}_2\text{O}_2$ , and blocked in 5% (v/v) BSA solution. Followed by enzymatic antigen retrieval, the sections were incubated with primary antibodies against COL I (NB600-450, Novus), COL II (NBP2-33343, Novus), COL X (ab58632, Abcam), AGG (ab3773, Abcam), and OCN (ab13418, Abcam). After rinsing with PBS, they were incubated with horseradish peroxidase-conjugated IgG, followed by 3, 3'-diaminobenzidine tetrahydrochloride (DAB) for visualization. Nuclei were counterstained with hematoxylin.

### 2.8. Quantitative reverse transcription-polymerase chain reaction (qRT-PCR)

The qRT-PCR was carried out to analyze specific genes for the bone-related markers COL I and OCN, as well as the cartilage-related markers aggrecan and COL II. For qRT-PCR, the entire defect regions were immediately harvested from the euthanized animals and quickly ground into powder under liquid nitrogen. Total RNA was extracted using TRIzol reagent (Invitrogen, USA) by following the standard procedures. Complementary DNAs (cDNAs) were synthesized from the total RNA, and qRT-PCR reactions were carried out and monitored with a Stratagene Mx3005P system (Stratagene, USA). The primer sequences of the targeted genes and the internal control gene  $\beta$ -actin are listed in Table S3. A difference in Ct values ( $\Delta\text{Ct}$ ) was calculated for each gene by triplicate, and the relative quantification of targeted genes was performed using the  $\Delta\Delta\text{Ct}$  method described previously [33].

### 2.9. Statistical analysis

The data were analyzed using SPSS version 22. Analytical

methods (Kolmogorov–Smirnov/Shapiro–Wilk test) were used to determine whether or not they were normally distributed. All quantitative data were expressed as mean  $\pm$  standard deviation. Statistical analysis was performed using one-way analysis of variance with *t*-test and a value of  $p < 0.05$  was considered to be

statistically significant. Statistical power analysis was calculated using Power and Sample Size Program. For histological scoring, the intraclass correlation coefficient (ICC) was employed to assess interobserver agreement.

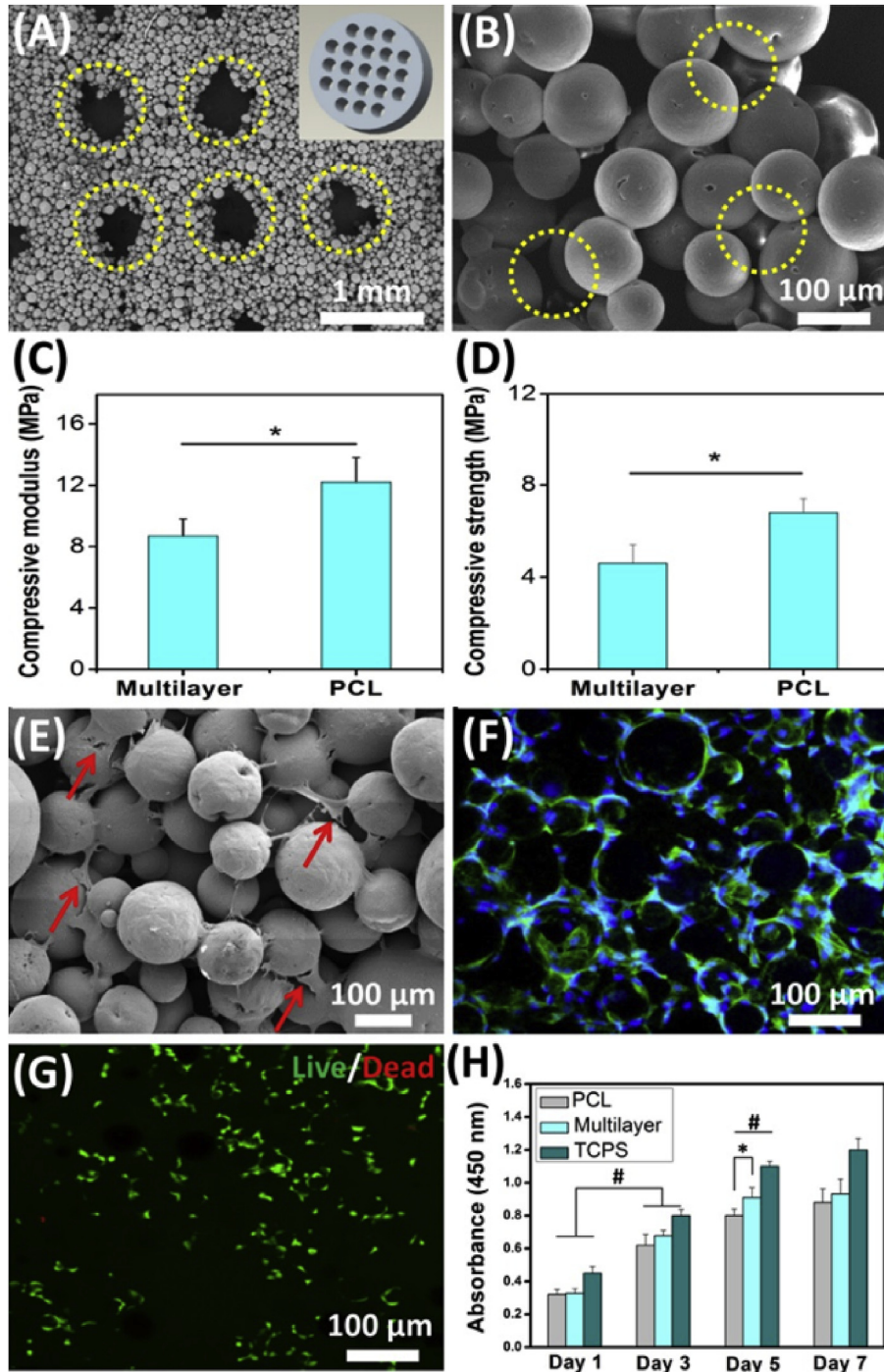


**Fig. 2. Characterization and *in vitro* cellular evaluation of SLS-derived scaffolds.** (A) The multilayer scaffold presented a macroporous structure (yellow circles) corresponding to the designed model (inset in A). (B) SEM image at high magnification further showed that a large number of micropores (yellow circles) were generated among the microspheres. (C, D) Both compressive modulus and compressive strength of the multilayer scaffold were less than those of the PCL scaffold. (E) SEM image showed that cells attached to the multilayer scaffold (red arrows). (F) Confocal fluorescence image further showed that the attached cells exhibited a normal morphology (green: cytoskeleton, blue: nuclei). (G) Live/dead assay verified that the multilayer scaffold could support cell viability after 7 days of culture (green: live cells, red: dead cells). (H) The scaffolds could support cell expansion. Tissue culture polystyrene (TCPS) was used as a control. Data are shown as mean  $\pm$  standard deviation for  $n = 5$ . (\*) indicates a significant difference between groups ( $p < 0.05$ ), (#) indicates a significant difference between day 1, day 3 and day 5 for the same group ( $p < 0.05$ ). (For interpretation of the references to colour in this figure legend, the reader is referred to the web version of this article.)

### 3. Results

#### 3.1. Characterization of SLS-derived multilayer scaffolds

Both the PCL microspheres and the HA/PCL composite microspheres presented a regular spherical shape with a diameter around 100  $\mu\text{m}$ . Meanwhile, the PCL microspheres exhibited a smooth surface whereas the HA/PCL composite microspheres were rough, and the roughness was enhanced with increased HA content (Fig. S2). Subsequently, the microspheres were used as building blocks to produce multilayer scaffolds via the SLS technique (Fig. 1B). It was worth noting that the vertical section of the multilayer scaffold clearly showed a continuous multilayer structure including the pure PCL layer (cartilage layer), composite layers of PCL with low HA content (transitional layer) and composite layers of PCL with high HA content (subchondral bone layer). Due to the continuous increase of HA content in each layer, the SEM images in Fig. 1B showed no obvious delamination in the transitional zone between the cartilage layer and subchondral bone layer. The multilayer scaffold showed a macroporous structure with the pore size range of 400–500  $\mu\text{m}$ , as designed before sintering (Fig. 2A). A large number of interconnected micropores were also present inside the scaffold due to the fusion of microspheres (Fig. 2B). The porosity of the multilayer scaffold was 60.3% and there was no statistical difference compared with the PCL scaffold (Fig. S3). The compressive modulus and compressive strength of the multilayer scaffold were 8.7 MPa and 4.6 MPa, respectively, significantly lower than those of the PCL scaffold (Fig. 2C and D). These results imply that the integration of HA reduces the mechanical properties of the multilayer scaffold. It is primarily due to the relative weak interaction between the HA particles and the PCL matrix. The HA particles on the surface of the microspheres significantly reduce the effective contact areas between the PCL matrix and lead to a relative weak connecting strength between the microspheres [30,41].

#### 3.2. In vitro cellular evaluation of SLS-derived scaffolds

Rat MSCs were used to evaluate the cell adhesion on SLS-derived multilayer scaffolds. It was found that the scaffolds were able to support cell adhesion, and the resident cells exhibited noticeably outspread pseudopods that were attached to the adjacent microspheres (Fig. 2E). Cells could also penetrate into the scaffold pores for further ingrowth. The fluorescent images clearly showed that the seeded cells distributed into the entire scaffold to form a highly interconnected cellular network (Fig. 2F). The cell viability was evaluated via live/dead assay and a large number of the resident cells exhibited a positive live staining after culturing for 7 days (Fig. 2G). Additionally, cell proliferation studies further showed that the cells grew fast on both the multilayer and the PCL scaffolds (Fig. 2H). After culturing for 5 days, the multilayer scaffolds showed a significant increase in cell number compared with the PCL scaffolds. Therefore, these findings suggest that the multilayer scaffolds present an excellent cytocompatibility *in vitro* and can support rMSCs adhesion and proliferation. In addition, the effect of HA content on cell adhesion and differentiation was investigated. The results showed that the cells could adhere on scaffolds with different HA contents (0–30%), and the HA content had no obvious influence on cell adhesion and migration (Fig. S4). However, SLS-derived HA/PCL scaffolds with HA content of 20–30% significantly increased the ALP activity of rMSCs (Fig. S5), which indicated that the HA gradient had an obvious influence on cell osteogenic differentiation.

#### 3.3. Superior repair in multilayer scaffolds by macroscopic observation

A rabbit model was used to evaluate the osteochondral repair capability for SLS-derived multilayer scaffolds (Fig. 3). Six weeks after implantation, the defects were filled with newly formed tissues in both the multilayer and the PCL scaffolds. Specifically,

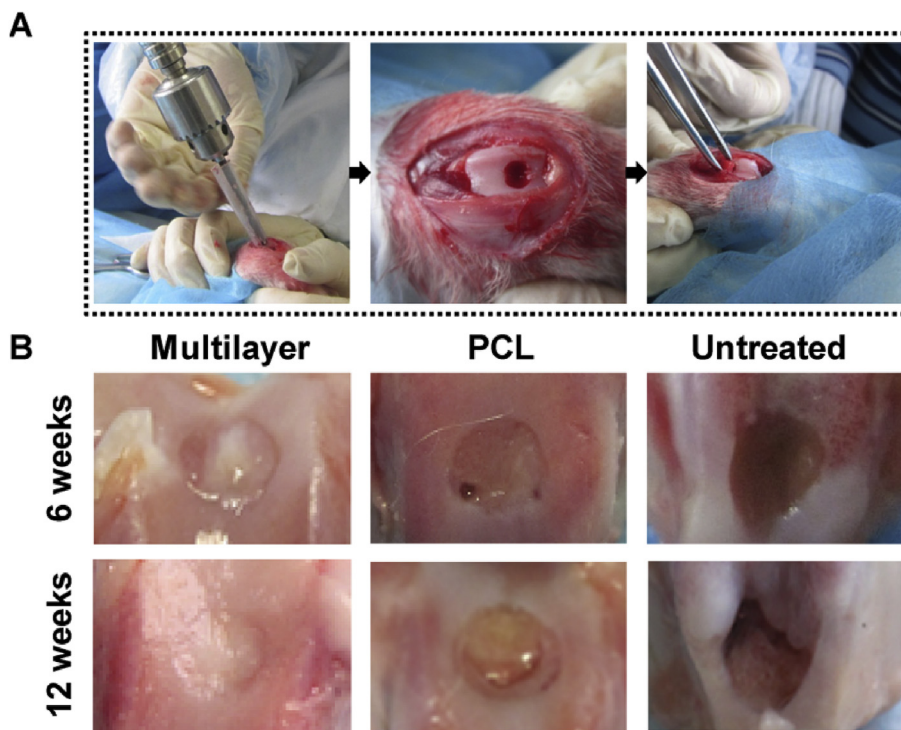


**Fig. 3.** *In vivo* evaluation of SLS-derived scaffolds. (A) Surgical procedures for creating an osteochondral defect model in rabbits. Defects were created using an orthopedic drill, and then different scaffolds were implanted. (B) Macroscopic observation at 6 and 12 weeks post-implantation showed that the cartilage repair in the multilayer scaffolds was superior to that in the PCL scaffolds and the untreated control. At week 12, the multilayer group displayed cartilage-like tissue with similar appearance to the surrounding native cartilage.

cartilage-like tissue was found in the multilayer scaffolds, while in the PCL scaffolds, only a small amount of cartilaginous tissue was found at the defect edge, with some small cavities. Additionally, there was no significant repair in the untreated control. Defect repair was enhanced with an increase in the implantation period from 6 weeks to 12 weeks. In particular, the formation of a smooth cartilage-like tissue with similar appearance to that of the adjacent native cartilage was observed in the multilayer scaffold group. However, the new-formed tissue was less transparent and there was an obvious boundary between the new tissue and native cartilage in the PCL group, an indication of incomplete repair. In contrast, there was even less tissue regenerated in the untreated defects and the surrounding host cartilage showed severe degradation.

### 3.4. Enhanced bone repair in multilayer scaffolds by micro-CT analysis

Micro-CT was further used to characterize the newly formed

tissue. The results demonstrated that the amount of new bone was much greater in the multilayer scaffolds than that in the PCL scaffolds at 6 weeks post implantation, and the same trend was shown for the thickness of corresponding trabecular bone (Fig. 4A). At week 12, defect sites in the multilayer group showed a high degree of new bone formation with thicker trabecular bone (Fig. 4B). In contrast, the bone repair in the PCL group was incomplete, with the new bone mainly distributed around the bottom and the side of the defects. For untreated defects, self-repair of subchondral bone was limited and there was a large cavity in the defect region. Compared with the other two groups, the multilayer group showed the highest bone volume per total volume (BV/TV) in both trabecular volume of interest (VOI) and cartilage and cortical (C&C) VOI for both 6- and 12-week time points (Fig. 4C). Similarly, bone mineral density (BMD) for both trabecular VOI and C&C VOI was significantly higher in the multilayer group than the other two groups (Fig. 4D). In addition, BV/TV and BMD also showed a time-dependent increase for each group.

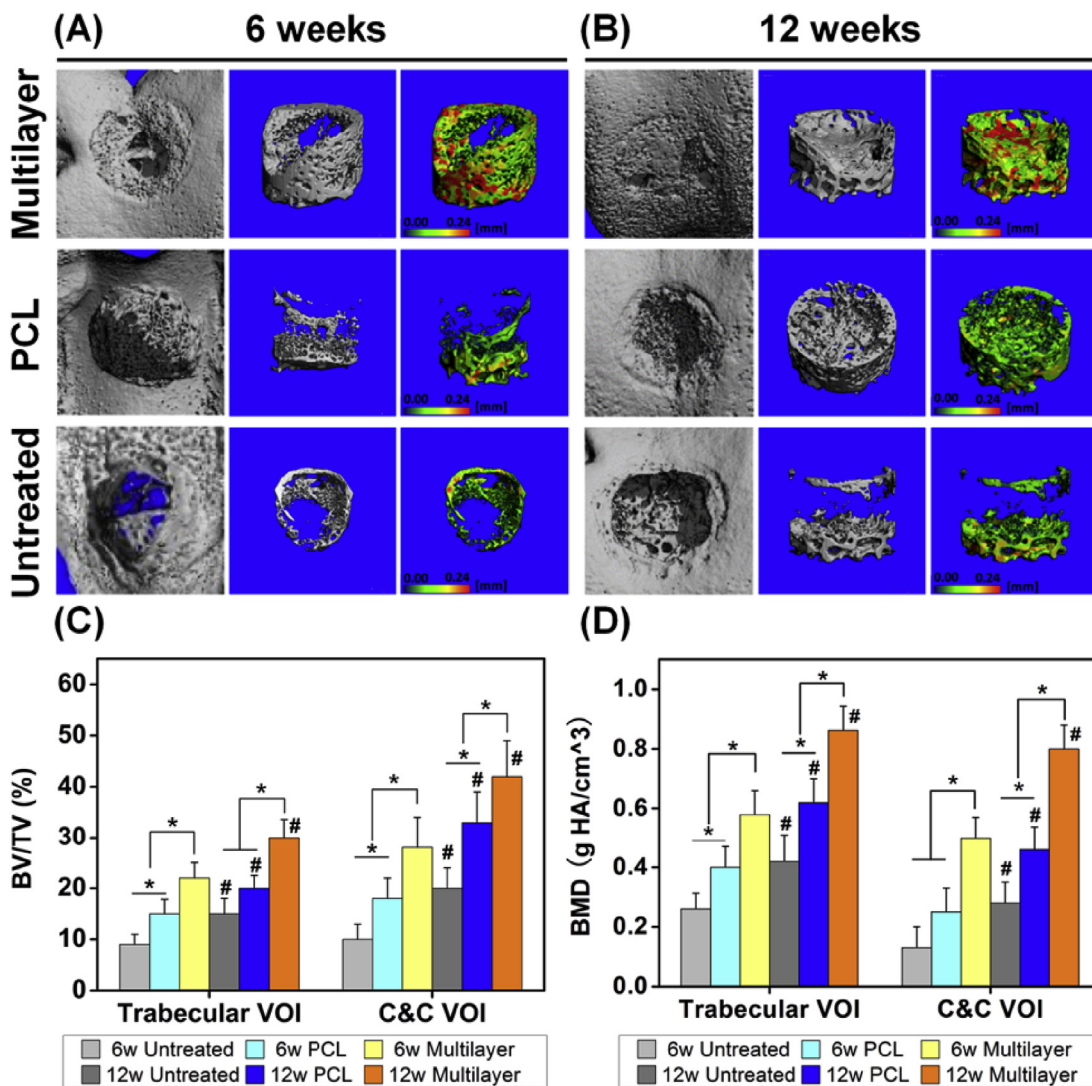


**Fig. 4.** Micro-CT analysis showed improved subchondral bone repair in multilayer scaffolds. (A, B) The reconstructed images showed the joint surfaces (the first column) and the regenerated bone in the defect area (the second column) at 6 and 12 weeks post-surgery. The pseudo-color images (the third column) showed the thickness of new trabecular bone in the range 0–0.24 mm, as indicated by the color changing from green to red. (C, D) The quantitative micro-CT data further demonstrated that the multilayer group had the highest bone volume per total volume (BV/TV) and bone mineral density (BMD), in both trabecular volume of interest (VOI) and cartilage and cortical (C&C) VOI. BV/TV and BMD also increased for each group with time. Data are shown as mean  $\pm$  standard deviation. (\*) indicates a significant difference between groups ( $p < 0.05$ ) and (#) indicates a significant difference between different time points for the same group ( $p < 0.05$ ). (For interpretation of the references to colour in this figure legend, the reader is referred to the web version of this article.)

3.5. Histological analysis: multilayer scaffolds promoted osteochondral repair

Histological staining analysis further confirmed that the multilayer scaffolds were able to enhance the repair of articular cartilage and subchondral bone, relative to the PCL scaffolds and the untreated control (Fig. 5). At 6 weeks post implantation, new cartilage in the multilayer scaffolds was observed at the edges of the defects, and new bone with hypertrophic cartilage was found in the subchondral region. Hematoxylin and eosin (H&E) staining at high

magnification showed evidence of new bone formation and neovascularization in the subchondral bone region of the multilayer scaffolds (Fig. S6). At 12 weeks post implantation, a layer of new cartilage was observed in the chondral region of the multilayer scaffolds, with a thickness similar to that of the adjacent cartilage. The new cartilage exhibited an intense staining of both safranin O-fast green (S-F) and toluidine blue (T-B), and was able to integrate with the adjacent cartilage. At high magnification, the chondrocyte arrangement in the new cartilage displayed a similar pattern to that of hyaline cartilage. In addition, there was more trabecular bone

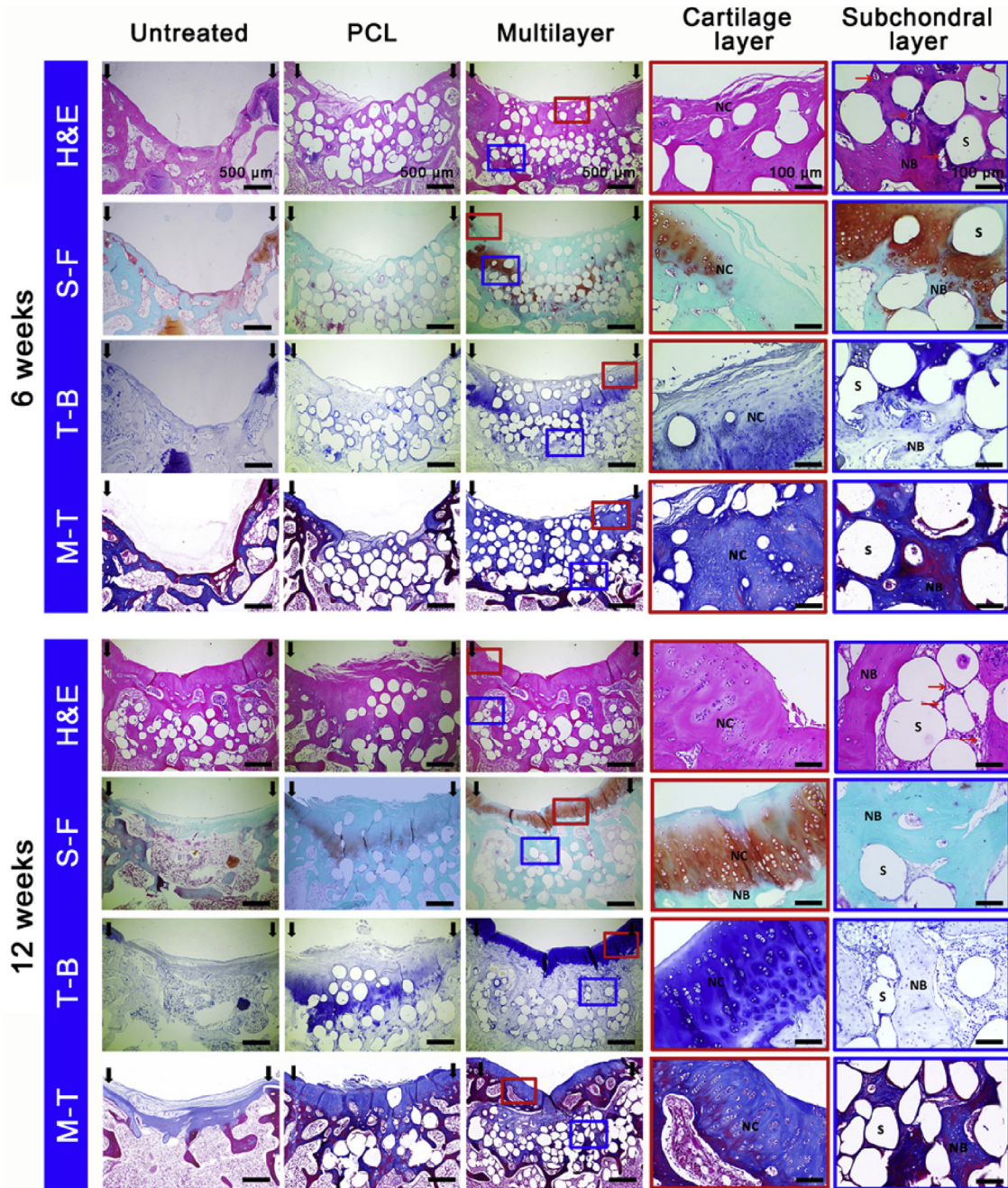


**Fig. 5. Histological analysis of tissue repair at 6 and 12 weeks post-surgery.** Hematoxylin and eosin (H&E), Safranin O-fast green (S-F), toluidine blue (T-B) and Masson's Tri-chrome (M-T) staining showed enhanced cartilage and subchondral bone repair in the multilayer group, compared to the PCL group and the untreated control. The enlarged images detailed the repair of cartilage layer and subchondral layer in the multilayer group. At week 6, new cartilage (NC) at the defect edges and new bone (NB) with hypertrophic cartilage in the subchondral region was observed. At week 12, both cartilage and subchondral bone were simultaneously repaired, with a well-integrated interface. S: scaffold, red arrows: new blood vessels.

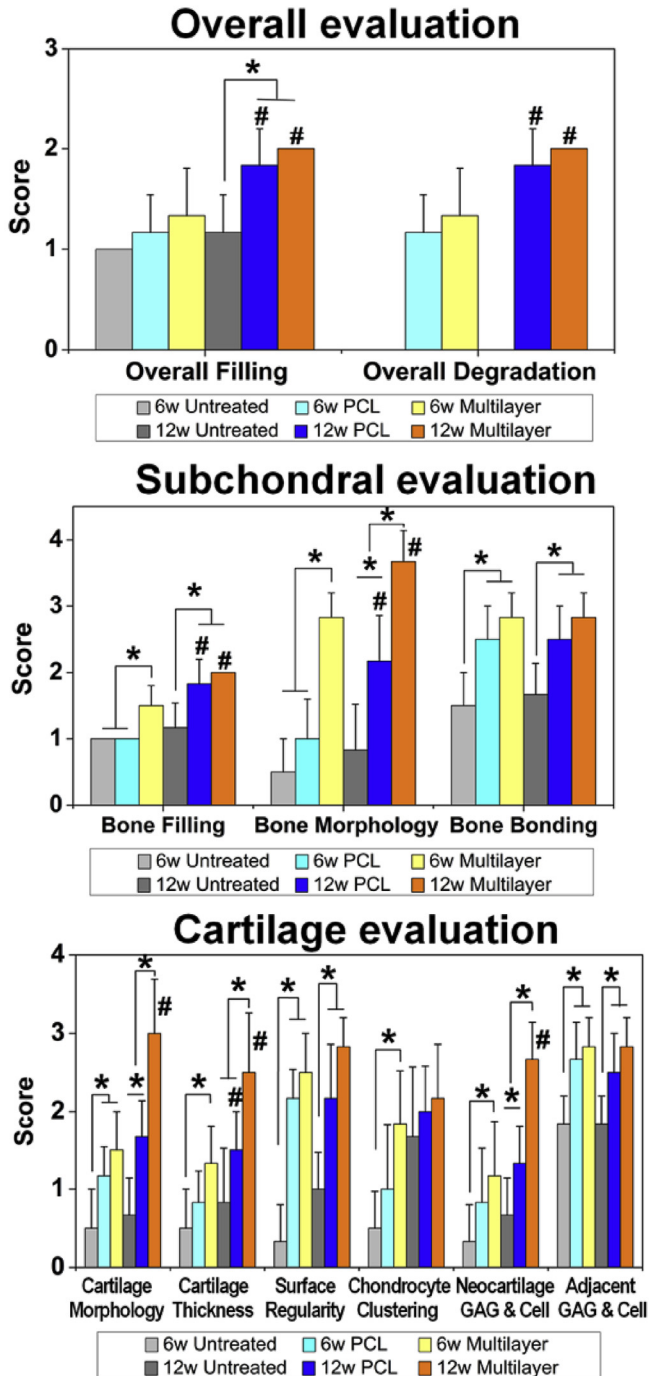


**Fig. 6. Histological score for the evaluation of osteochondral repair.** The data showed that the overall tissue filling was improved with implantation time in both scaffold groups. The multilayer group got significantly higher scores than the PCL group on both bone filling and bone morphology in the subchondral bone region (at week 6), as well as cartilage morphology, cartilage thickness, and glycosaminoglycan & chondrocyte content (GAG & Cell) of neocartilage in the cartilage region (at week 12). Data are shown as mean  $\pm$  standard deviation. (\*) indicates a significant difference between groups ( $p < 0.05$ ), (#) indicates a significant difference between different time points for the same group ( $p < 0.05$ ). The value of the intraclass correlation coefficient (ICC) was 0.853.

regenerated in the subchondral bone region of the multilayer scaffolds. A well-integrated interface between the regenerated articular cartilage and the subchondral bone was also observed, with no evidence of bone overgrowth towards the cartilage region (Fig. S7).

In comparison, defects treated with the PCL scaffolds showed limited bone and cartilage repair with poor quality for up to 12 weeks (Fig. S8), while empty cavities and scarce regenerated tissue were present in the untreated defects, with the collapse of adjacent cartilage (Fig. S9). The Masson's trichrome (M-T) staining further showed that the collagen secretion was enhanced in the multilayer group, compared with the PCL group and the untreated control.

A quantitative scoring for the histological staining, regarding the overall defect evaluation, subchondral bone evaluation and articular cartilage evaluation, was further performed (Fig. 6). Both the overall tissue filling and overall implant degradation in the two scaffold groups increased with implantation time, and the two parameters had the same scores, which suggested a dynamic balance between tissue filling and scaffold degradation. As for evaluation of subchondral bone, the multilayer scaffolds showed the highest scores on the bone filling and bone morphology at 6 weeks post implantation. At 12 weeks post implantation, the bone filling and bone morphology scores in both scaffold groups increased and the bone morphology score of the multilayer group remained the highest. It was also noticeable that the implanted scaffolds significantly enhanced the bone bonding compared to the untreated control. For evaluation of articular cartilage, the multilayer scaffolds showed the highest scores on cartilage morphology, cartilage thickness, as well as the glycosaminoglycan (GAG) & chondrocyte content of neocartilage at week 12, and these scores were significantly higher than those at week 6. In addition, both scaffold groups showed significantly higher scores on cartilage morphology, joint surface regularity and GAG & chondrocyte content of adjacent cartilage than the untreated control.

### 3.6. Immunohistochemical staining for both cartilage and bone-specific proteins

Immunohistochemical (IHC) staining for both cartilage and bone-specific proteins was carried out to further evaluate the osteochondral repair. AGG and COL II were positively stained in both scaffold groups, and the protein expressions were increased with time (Fig. 7). Furthermore, the positively stained regions matched with those in S-F and T-B staining. Enlarged images of COL II staining at week 12 showed that the multilayer scaffolds induced formation of hyaline-like cartilage with typical elongated chondrocytes that embedded in lacunae. It was worth noting that the staining for these two proteins was much stronger in the multilayer group than that in the PCL group and the untreated control (Fig. S10). COL X is indicative of hypertrophy, and it was expressed at week 6 in the subchondral bone region, indicating that some of the chondrocytes were exhibiting a hypertrophic phenotype for tissue calcification. However, COL X almost disappeared in the cartilage layer of the multilayer group, indicating the formation of hyaline cartilage at week 12. To evaluate the subchondral bone repair, IHC staining of OCN and COL I was carried out (Fig. 8). Both proteins were positively stained at the subchondral bone region, with a time-dependent increase in staining intensity. There was negligible OCN or COL I distributed in neo-cartilage layer. At each time point, the staining for these two proteins was remarkably stronger in the multilayer group than that in the PCL group and the untreated control (Fig. S10), indicating an enhanced subchondral bone regeneration.

### 3.7. Up-regulation of chondrogenesis and osteogenesis genes in the multilayer group

Relative mRNA levels for chondrogenesis and osteogenesis genes in the multilayer and PCL groups were evaluated with qRT-PCR (Fig. 9). At 12 weeks post implantation, the chondrogenesis

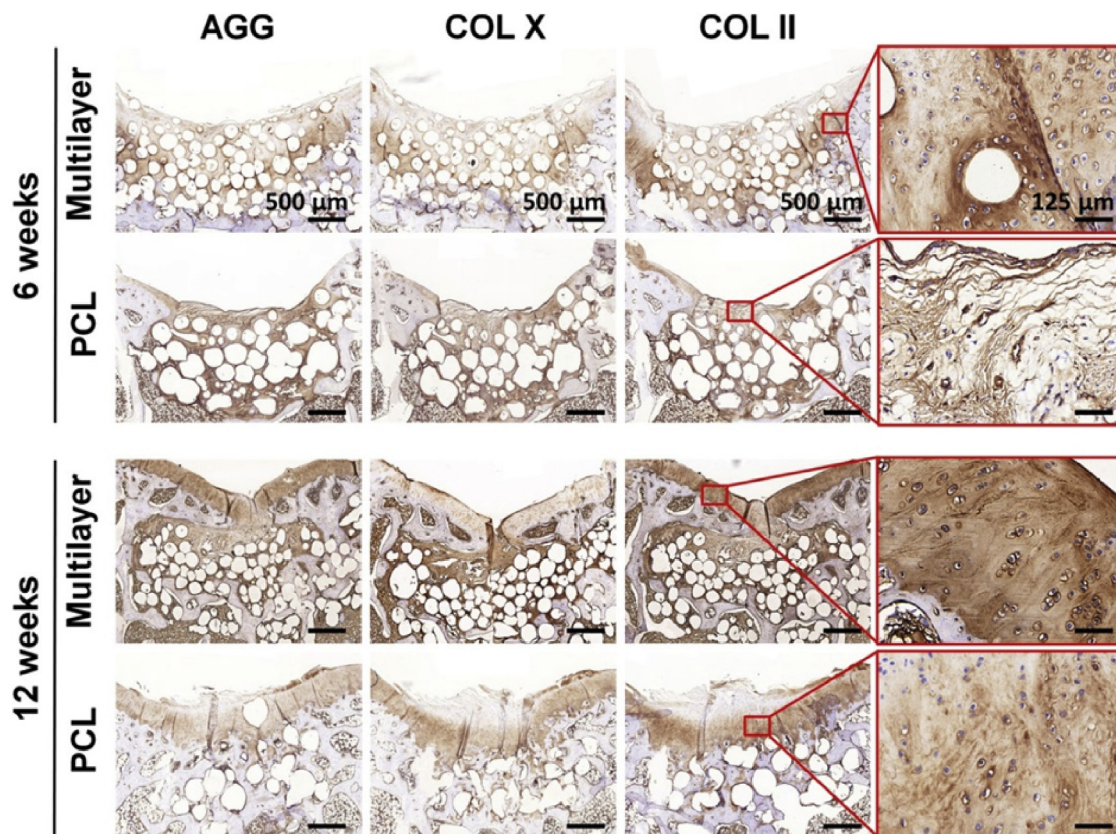


**Fig. 7. Immunohistochemical staining for cartilage-specific proteins.** Aggrecan (AGG), collagen type X (COL X), and collagen type II (COL II) in sections from the multilayer and PCL groups were visualized at week 6 and week 12. Both AGG and COL II were abundant in the new cartilage of the multilayer group at week 12, and the expression of COL X was relatively low. The enlarged images of the selected region showed the distribution of COL II.

genes such as aggrecan and COL II were upregulated in both scaffold groups, and their expressions in the multilayer group were significantly higher than those in the PCL group. Similarly, osteogenesis-associated genes including COL I and OCN were also upregulated in the multilayer group compared with the PCL group and the untreated control.

#### 4. Discussion

Due to the complex hierarchical architecture of osteochondral tissue, highly bio-inspired multilayer scaffolds are potentially required as regenerative grafts [42]. However, the design of scaffolds that reflects the complexity of the osteochondral unit, with the robust integration of the cartilage and bone, is particularly challenging. In this study, we constructed a multilayer scaffold with a continuous HA gradient, which was advantageous for continuous transition of component between each layer (Fig. 1). Moreover, instead of traditional techniques [17,43,44], SLS was employed for the fabrication of scaffolds due to its innate advantages in the rapid manufacturing of lamellar structure, the precise control of sophisticated design, and the potential for mass production. The application of SLS technique creatively overcomes the drawbacks of traditional methods, including restrictions on layer number, limited control of hierarchical structure, unexpected separation between the layers, and poor connective porosity. Therefore, using SLS technique to construct the multilayer osteochondral scaffold is a major innovation in this study.

In addition to replicating the structural complexity, bio-inspired scaffolds need to provide suitable mechanical support to avoid collapse and depression of newly formed tissues, while promoting

the osteochondral regeneration [45]. To achieve these goals, the PCL and HA/PCL composite microspheres were applied as building blocks for SLS to produce the multilayer scaffolds. PCL is a biodegradable polymer that has been extensively used in the field of tissue engineering due to its tailored mechanical properties, and HA is used to increase the osteoconductive capacity. Compared to osteochondral scaffolds in other studies [17,20], the microsphere-based HA/PCL scaffolds fabricated in this study showed superior mechanical performance, with compressive modulus and compressive strength of the multilayer scaffolds reaching 8.7 and 4.6 MPa, respectively (Fig. 2C–D), at the porosity of 60%. In addition, the continuous gradient distribution of HA across each layer can address the layer separation issue that frequently took place in traditional bilayered scaffolds.

Along with the advantages in scaffold composition, the macro/microporous structure throughout the scaffold (Fig. 2A–B) formed by the SLS process can support cell migration and cell attachment *in vitro* (Fig. 2E–H). Instead of blending bioceramic particles and polymer powders directly in conventional SLS strategies [41,46,47], using the HA/PCL composite microspheres with regular shape and better mobility enhanced the precision and connective porosity during the SLS process [30,48]. In addition, the interconnected macro/micropores allow rapid cell migration from the marrow space up to the joint surface immediately after the *in vivo* implantation, and also facilitate the chondrogenesis, angiogenesis and bone tissue infiltration throughout the *in vivo* regeneration.

Animal experiments demonstrated an improved repair for both the subchondral bone and articular cartilage in SLS-derived scaffolds, compared to the spontaneous healing process in the untreated group (Figs. 3–6). Although both the multilayer and the PCL

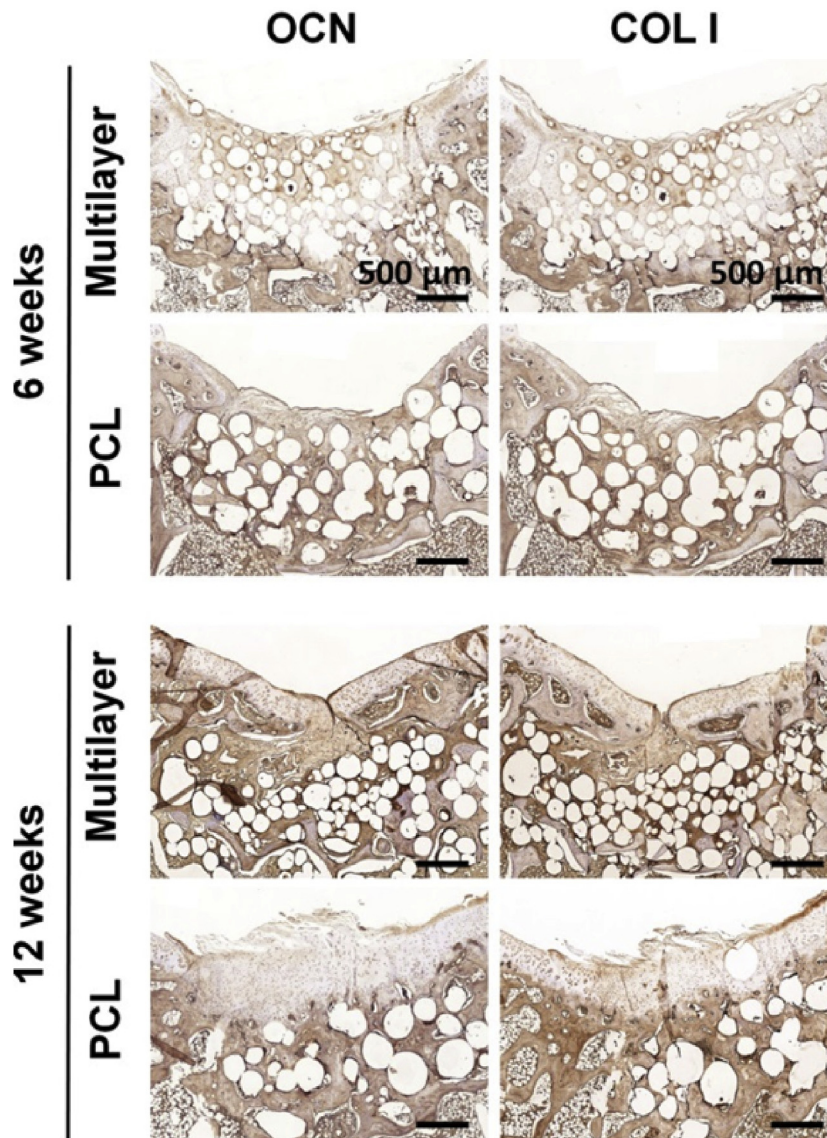


**Fig. 8.** Immunohistochemical staining for bone-specific proteins. Osteocalcin (OCN) and collagen type I (COL I) in sections from the multilayer and PCL groups were visualized at week 6 and week 12. The subchondral bone region was enriched with OCN and COL I, and the staining for both proteins was remarkably stronger in the multilayer group than that in the PCL group.

scaffolds can facilitate osteochondral repair, the performance of the multilayer scaffolds was superior to the PCL scaffolds. This was partly due to the HA gradient in the multilayer scaffolds accelerated the early regeneration of subchondral bone and enhanced the stable integration between the new bone and native bone. The *in vitro* cell experiment also indicated that the HA gradient had an obvious influence on osteogenic differentiation (Fig. S5). Both the micro-CT and histological analysis clearly demonstrated that a large amount of new bone was formed throughout the multilayer scaffolds at 6 weeks post implantation, resulting a higher score of early bone repair. This newly formed bone integrated well with the adjacent native bone and thus provided a stable anchoring of the graft within the defect [49].

These findings are important because subchondral bone is considered as a key foundation for successful articular cartilage repair, while an inferior repair of subchondral bone will decrease the biomechanical properties of the entire osteochondral area and negatively impact the long-term performance of the cartilaginous repair tissue [50,51]. Histological analysis demonstrated a high

quality of cartilage repair in the multilayer group at week 12 (Figs. 5–7). qRT-PCR study for the newly formed tissue also showed higher levels of chondrogenesis gene expressions in the multilayer group, compared with those in the PCL group (Fig. 9). These findings are consistent with previous studies [52], and verify that early bone repair facilitates the corresponding cartilage regeneration. Thus, the HA gradient in the multilayer scaffolds is indeed a crucial factor in promoting the regeneration of osteochondral tissue by accelerating the early subchondral bone repair.

Another interesting finding is the gradually moving up of the neo-cartilage band towards the joint surface as indicated by the S-F and T-B staining, from week 6 to week 12 (Fig. 5). After scaffolds were implanted into osteochondral defects, the post-injury response involved a rapid influx of host MSCs and growth factors into the defect area and the fabrication of embryonic-like cartilage tissue throughout the defects [40]. Neo-cartilage was observed in the subchondral area, indicative of the process of cartilage resorption and bone formation. Specifically, in the bony region of the scaffolds, the incorporation of HA promoted the ossification,

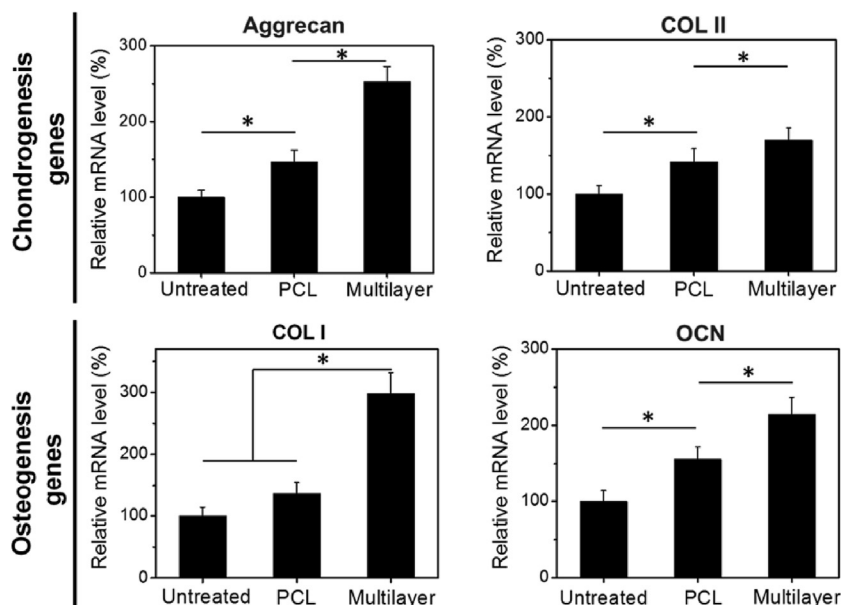


**Fig. 9.** Gene analysis for chondrogenesis and osteogenesis in newly formed tissue at week 12. qRT-PCR results demonstrated that the multilayer group showed the highest expression of cartilage-associated genes, such as aggrecan and collagen type II (COL II), as well as the osteogenesis-associated genes, such as collagen type I (COL I) and osteocalcin (OCN). Data are shown as mean  $\pm$  standard deviation for  $n = 3$ . (\*) indicates a significant difference between groups ( $p < 0.05$ ).

with chondrocyte hypertrophy and vascular invasion. The ossification process started from the bottom of the defect and gradually moved up, resulting the gradually moving up of the neo-cartilage band towards the joint surface.

The osteochondral interface that connects the cartilage and bone, plays an important role in maintaining the structural integrity of the articular cartilage [53]. In addition to subchondral bone and articular cartilage regeneration, excellent reconstruction of the osteochondral interface was observed in the multilayer scaffolds at 12 weeks post implantation (Fig. S7). The osteochondral regeneration was mediated by endochondral ossification, and in current study the cartilaginous tissue was developed from the deep region of the defects (Fig. 5), where there was adequate calcium stimulation signaling, and sufficient stem-cells source and nutrients supply from the adjacent subchondral bone. The cartilage thickness and location were determined synergistically by the continuous chondrogenesis towards the outer surface (positive regulation) and advancement of tidemark mineralization front (negative regulation) [14,54]. In this study, histological staining results showed that abundant cartilaginous tissue was generated and the tidemark was gradually developing, only in the multilayer scaffolds at week 6. The chondrogenesis front as well as the tidemark in this group became clear and advanced outwards at week 12, thinning the cartilage to a normal thickness and shifting it to the surface of the defects (Fig. 5). However, these results were not duplicated in either the PCL or the untreated group. An intermediate osteochondral layer within scaffolds is advantageous to the restoration of the anatomical tidemark in rabbit and caprine joints [44,55]. The current work showed the similar results, and demonstrated that the precise control of the thickness and HA content in each scaffold layer contributed to the integrated reconstruction of osteochondral interface.

Therefore, such well-designed multilayer scaffold, which mimics the hierarchical complexity of the osteochondral unit, not only encourages fast subchondral bone repair, but also promotes articular cartilage regeneration and induces the formation of an integrated osteochondral interface. For the potential clinic application, the technology could be scaled up to humans by modifying the scaffold model design to adapt the different dimension and thickness for human knee defects. Due to its controllable forming process, flexible

structural design, tailored composition, and tunable biomechanical properties, this scaffold provides an ideal platform for the enhanced repair of osteochondral defects.

## 5. Conclusion

In summary, a biomimetic osteochondral scaffold with continuous multilayer architecture and gradient composition from articular cartilage layer to subchondral bone layer was fabricated using a microsphere-based SLS technique. Our results demonstrated that the resultant multilayer scaffold featured highly interconnected porosity and desirable mechanical properties as well as excellent biocompatibility. *In vivo* animal evaluation further verified that the multilayer scaffold could successfully induce osteochondral repair, and that the newly formed tissue manifested multiple tissues types including articular cartilage and subchondral bone. Consequently, the current work greatly advances the potential application of SLS technique towards regenerative medicine by producing bio-inspired multilayer scaffolds for comprehensive osteochondral repair.

## Acknowledgements

This work was supported by grants from the National Natural Science Foundation of China (81461148032 and 31430029), HUST Key Innovation Team Project for Interdisciplinary Advancement (2016JCTD101), the National Research Foundation of Korea (2014K2A2A7060928), and the National Institutes of Health of the United States (R01 AR068073). We thank Jason Guo, Yuseon Kim, and Gerry Koons for their assistance in the preparation of the manuscript.

## Appendix A. Supplementary data

Supplementary data related to this article can be found at <http://dx.doi.org/10.1016/j.biomaterials.2017.05.021>.

## References

- [1] B.R. Mandelbaum, J.E. Browne, F. Fu, L. Micheli, J.B. Mosely, C. Erggelet, et al.,

- Articular cartilage lesions of the knee, *Am. J. Sports Med.* 26 (1998) 853–861.
- [2] E.B. Hunziker, Articular cartilage repair: basic science and clinical progress. A review of the current status and prospects, *Osteoarthr. Cartil.* 10 (2002) 432–463.
- [3] D.J. Huey, J.C. Hu, K.A. Athanasiou, Unlike bone, cartilage regeneration remains elusive, *Science* 338 (2012) 917–921.
- [4] G.D. Smith, G. Knutsen, J.B. Richardson, A clinical review of cartilage repair techniques, *J. Bone Jt. Surg. Br.* 87 (2005) 445–449.
- [5] M. Marcacci, E. Kon, M. Delcogliano, G. Filardo, M. Busacca, S. Zaffagnini, Arthroscopic autologous osteochondral grafting for cartilage defects of the knee: prospective study results at a minimum 7-year follow-up, *Am. J. Sports Med.* 35 (2007) 2014–2021.
- [6] G.M. Salzmann, M. Sauerschnig, M.T. Berninger, T. Kaltenhauser, M. Schonfelder, S. Vogt, et al., The dependence of autologous chondrocyte transplantation on varying cellular passage, yield and culture duration, *Biomaterials* 32 (2011) 5810–5818.
- [7] G. Filardo, F. Vannini, M. Marcacci, L. Andriolo, A. Ferruzzi, S. Giannini, et al., Matrix-assisted autologous chondrocyte transplantation for cartilage regeneration in osteoarthritic knees: results and failures at midterm follow-up, *Am. J. Sports Med.* 41 (2013) 95–100.
- [8] M. Eldracher, P. Orth, M. Cucchiari, D. Pape, H. Madry, Small subchondral drill holes improve marrow stimulation of articular cartilage defects, *Am. J. Sports Med.* 42 (2014) 2741–2750.
- [9] A. Gobbi, G. Karnatzikos, A. Kumar, Long-term results after microfracture treatment for full-thickness knee chondral lesions in athletes, *Knee Surg. Sports Traumatol. Arthrosc.* 22 (2014) 1986–1996.
- [10] L. Hangody, J. Dobos, E. Baló, G. Panics, L.R. Hangody, I. Berkes, Clinical experiences with autologous osteochondral mosaicplasty in an athletic population: a 17-year prospective multicenter study, *Am. J. Sports Med.* 38 (2010) 1125–1133.
- [11] J.S. Temenoff, A.G. Mikos, Review: tissue engineering for regeneration of articular cartilage, *Biomaterials* 21 (2000) 431–440.
- [12] H.S. Yang, W.G. La, S.H. Bhang, H.J. Kim, G.I. Im, H. Lee, et al., Hyaline cartilage regeneration by combined therapy of microfracture and long-term bone morphogenetic protein-2 delivery, *Tissue Eng. Part A* 17 (2011) 1809–1818.
- [13] N. Mahmoudifar, P.M. Doran, Tissue engineering of human cartilage and osteochondral composites using recirculation bioreactors, *Biomaterials* 26 (2005) 7012–7024.
- [14] A. Tampieri, M. Sandri, E. Landi, D. Pressato, S. Francioli, R. Quarto, et al., Design of graded biomimetic osteochondral composite scaffolds, *Biomaterials* 29 (2008) 3539–3546.
- [15] X. Guo, H. Park, G. Liu, W. Liu, Y. Cao, Y. Tabata, et al., In vitro generation of an osteochondral construct using injectable hydrogel composites encapsulating rabbit marrow mesenchymal stem cells, *Biomaterials* 30 (2009) 2741–2752.
- [16] S.P. Nukavarapu, D.L. Dorcenus, Osteochondral tissue engineering: current strategies and challenges, *Biotechnol. Adv.* 31 (2013) 706–721.
- [17] L.P. Yan, J. Silva-Correia, M.B. Oliveira, C. Vilela, H. Pereira, R.A. Sousa, et al., Bilayered silk/silk-nanoCaP scaffolds for osteochondral tissue engineering: in vitro and in vivo assessment of biological performance, *Acta Biomater.* 12 (2015) 227–241.
- [18] T. Gotterbarm, W. Richter, M. Jung, S. Berardi Vilei, P. Mainil-Varlet, T. Yamashita, et al., An in vivo study of a growth-factor enhanced, cell free, two-layered collagen-tricalcium phosphate in deep osteochondral defects, *Biomaterials* 27 (2006) 3387–3395.
- [19] J.M. Oliveira, M.T. Rodrigues, S.S. Silva, P.B. Malafaya, M.E. Gomes, C.A. Viegas, et al., Novel hydroxyapatite/chitosan bilayered scaffold for osteochondral tissue engineering applications: scaffold design and its performance when seeded with goat bone marrow stromal cells, *Biomaterials* 27 (2006) 6123–6137.
- [20] T.J. Levingstone, A. Matsiko, G.R. Dickson, F.J. O'Brien, J.P. Gleeson, A biomimetic multi-layered collagen-based scaffold for osteochondral repair, *Acta Biomater.* 10 (2014) 1996–2004.
- [21] P.E. Muller, F. Schrimpf, S. Milz, J. Kircher, H.R. Durr, B. Wegener, et al., Repair of osteochondral defects in the knee by resorbable bioimplants in a rabbit model, *Acta Orthop.* 77 (2006) 981–985.
- [22] J.M. Williams, A. Adewunmi, R.M. Schek, C.L. Flanagan, P.H. Krebsbach, S.E. Feinberg, et al., Bone tissue engineering using polycaprolactone scaffolds fabricated via selective laser sintering, *Biomaterials* 26 (2005) 4817–4827.
- [23] W.Y. Yeong, N. Sudarmadji, H.Y. Yu, C.K. Chua, K.F. Leong, S.S. Venkatraman, et al., Porous polycaprolactone scaffold for cardiac tissue engineering fabricated by selective laser sintering, *Acta Biomater.* 6 (2010) 2028–2034.
- [24] F.E. Wiria, K.F. Leong, C.K. Chua, Y. Liu, Poly-epsilon-caprolactone/hydroxyapatite for tissue engineering scaffold fabrication via selective laser sintering, *Acta Biomater.* 3 (2007) 1–12.
- [25] K.F. Leong, C.M. Cheah, C.K. Chua, Solid freeform fabrication of three-dimensional scaffolds for engineering replacement tissues and organs, *Biomaterials* 24 (2003) 2363–2378.
- [26] S.J. Hollister, Porous scaffold design for tissue engineering, *Nat. Mater.* 4 (2005) 518–524.
- [27] S. Kumar, Selective laser sintering: a qualitative and objective approach, *J. Min. Met. Mater. Soc.* 55 (2003) 43–47.
- [28] M.A. Woodruff, D.W. Hutmacher, The return of a forgotten polymer—polycaprolactone in the 21st century, *Prog. Polym. Sci.* 35 (2010) 1217–1256.
- [29] C.H. Chen, M.Y. Lee, V.B. Shyu, Y.C. Chen, C.T. Chen, J.P. Chen, Surface modification of polycaprolactone scaffolds fabricated via selective laser sintering for cartilage tissue engineering, *Mater. Sci. Eng. C* 40 (2014) 389–397.
- [30] Y. Du, H. Liu, J. Shuang, J. Wang, J. Ma, S. Zhang, Microsphere-based selective laser sintering for building macroporous bone scaffolds with controlled microstructure and excellent biocompatibility, *Colloids Surf. B. Biointerfaces* 135 (2015) 81–89.
- [31] J. Liu, Z. Qiu, S. Wang, L. Zhou, S. Zhang, A modified double-emulsion method for the preparation of daunorubicin-loaded polymeric nanoparticle with enhanced in vitro anti-tumor activity, *Biomed. Mater.* 5 (2010) 065002.
- [32] Z.Y. Qiu, G. Li, Y.Q. Zhang, J. Liu, W. Hu, J. Ma, et al., Fine structure analysis and sintering properties of Si-doped hydroxyapatite, *Biomed. Mater.* 7 (2012) 045009.
- [33] J. Wang, Q. Yang, C. Mao, S. Zhang, Osteogenic differentiation of bone marrow mesenchymal stem cells on the collagen/silk fibroin bi-template-induced biomimetic bone substitutes, *J. Biomed. Mater. Res. A* 100 (2012) 2929–2938.
- [34] Y. Wang, J. Wang, H. Hao, M. Cai, S. Wang, J. Ma, et al., Vitro and in vivo mechanism of bone tumor inhibition by selenium-doped bone mineral nanoparticles, *ACS Nano* 10 (2016) 9927–9937.
- [35] J. Yang, G. Shi, J. Bei, S. Wang, Y. Cao, Q. Shang, et al., Fabrication and surface modification of macroporous poly(L-lactic acid) and poly(L-lactic-co-glycolic acid) (70/30) cell scaffolds for human skin fibroblast cell culture, *J. Biomed. Mater. Res.* 62 (2002) 438–446.
- [36] ASTM D 1621–10, Standard Test Method for Compressive Properties of Rigid Cellular Plastics.
- [37] L. Ardeshirpour, S. Brian, P. Dann, J. VanHouten, J. Wysolmerski, Increased PTHrP and decreased estrogens alter bone turnover but do not reproduce the full effects of lactation on the skeleton, *Endocrinology* 151 (2010) 5591–5601.
- [38] J. Lam, S. Lu, E.J. Lee, J.E. Trachtenberg, V.V. Meretoja, R.L. Dahlin, et al., Osteochondral defect repair using bilayered hydrogels encapsulating both chondrogenically and osteogenically pre-differentiated mesenchymal stem cells in a rabbit model, *Osteoarthr. Cartil.* 22 (2014) 1291–1300.
- [39] S. Lu, J. Lam, J.E. Trachtenberg, E.J. Lee, H. Seyednejad, J.J. van den Beucken, et al., Dual growth factor delivery from bilayered, biodegradable hydrogel composites for spatially-guided osteochondral tissue repair, *Biomaterials* 35 (2014) 8829–8839.
- [40] X. Guo, H. Park, S. Young, J.D. Kretlow, J.J. van den Beucken, L.S. Baggett, et al., Repair of osteochondral defects with biodegradable hydrogel composites encapsulating marrow mesenchymal stem cells in a rabbit model, *Acta Biomater.* 6 (2010) 39–47.
- [41] S. Eosoly, N.E. Vrana, S. Lohfeld, M. Hindie, L. Looney, Interaction of cell culture with composition effects on the mechanical properties of polycaprolactone-hydroxyapatite scaffolds fabricated via selective laser sintering (SLS), *Mater. Sci. Eng. C* 32 (2012) 2250–2257.
- [42] S. Lopa, H. Madry, Bioinspired scaffolds for osteochondral regeneration, *Tissue Eng. Part A* 20 (2014) 2052–2076.
- [43] C. Sosio, A. Di Giancamillo, D. Deponti, F. Gervaso, F. Scalera, M. Melato, et al., Osteochondral repair by a novel interconnecting collagen-hydroxyapatite substitute: a large-animal study, *Tissue Eng. Part A* 21 (2015) 704–715.
- [44] T.J. Levingstone, A. Ramesh, R.T. Brady, P.A. Brama, C. Kearney, J.P. Gleeson, et al., Cell-free multi-layered collagen-based scaffolds demonstrate layer specific regeneration of functional osteochondral tissue in caprine joints, *Biomaterials* 87 (2016) 69–81.
- [45] I. Martin, S. Miot, A. Barbero, M. Jakob, D. Wendt, Osteochondral tissue engineering, *J. Biomech.* 40 (2007) 750.
- [46] S. Lohfeld, S. Cahill, V. Barron, P. McHugh, L. Durselen, L. Kreja, et al., Fabrication, mechanical and in vivo performance of polycaprolactone/tricalcium phosphate composite scaffolds, *Acta Biomater.* 8 (2012) 3446–3456.
- [47] Y. Xia, P. Zhou, X. Cheng, Y. Xie, C. Liang, C. Li, et al., Selective laser sintering fabrication of nano-hydroxyapatite/poly-epsilon-caprolactone scaffolds for bone tissue engineering applications, *Int. J. Nanomed.* 8 (2013) 4197–4213.
- [48] B. Duan, M. Wang, W.Y. Zhou, W.L. Cheung, Z.Y. Li, W.W. Lu, Three-dimensional nanocomposite scaffolds fabricated via selective laser sintering for bone tissue engineering, *Acta Biomater.* 6 (2010) 4495–4505.
- [49] P.B. Malafaya, R.L. Reis, Bilayered chitosan-based scaffolds for osteochondral tissue engineering: influence of hydroxyapatite on in vitro cytotoxicity and dynamic bioactivity studies in a specific double-chamber bioreactor, *Acta Biomater.* 5 (2009) 644–660.
- [50] H. Madry, The subchondral bone: a new frontier in articular cartilage repair, *Knee Surg. Sports Traumatol. Arthrosc.* 18 (2010) 417–418.
- [51] P. Orth, M. Cucchiari, D. Kohn, H. Madry, Alterations of the subchondral bone in osteochondral repair - translational data and clinical evidence, *Eur. Cell Mater.* 25 (2013) 299–316.
- [52] N. Mohan, N.H. Dormer, K.L. Caldwell, V.H. Key, C.J. Berklund, M.S. Detamore, Continuous gradients of material composition and growth factors for effective regeneration of the osteochondral interface, *Tissue Eng. Part A* 17 (2011) 2845–2855.
- [53] N.T. Khanarian, N.M. Haney, R.A. Burga, H.H. Lu, A functional agarose-hydroxyapatite scaffold for osteochondral interface regeneration, *Biomaterials* 33 (2012) 5247–5258.
- [54] K.M. O'Connor, Unweighting accelerates tidemark advancement in articular cartilage at the knee joint of rats, *J. Bone Min. Res.* 12 (1997) 580–589.
- [55] T.J. Levingstone, E. Thompson, A. Matsiko, A. Schepens, J.P. Gleeson, F.J. O'Brien, Multi-layered collagen-based scaffolds for osteochondral defect repair in rabbits, *Acta Biomater.* 32 (2016) 149–160.